Hes1 oscillations synchronize and refine condensation formation and patterning of the avian limb skeleton

Ramray Bhat[1], Tilmann Glimm[2], Marta Linde-Medina[3,4], Cheng Cui[3], Stuart A. Newman[3]

[1] Department of Molecular Reproduction, Development and Genetics, Biological Sciences Division, Indian Institute of Science, Bangalore, 560012, India

[2] Department of Mathematics, Western Washington University, Bellingham, WA 98229, USA

[3] Department of Cell Biology and Anatomy, New York Medical College, Valhalla, NY 10595 USA

[4] Current address: Department of Orthopaedic Surgery, San Francisco General Hospital, Orthopaedic Trauma Institute, University of California, San Francisco, CA 94110, USA

Abstract

The tetrapod appendicular skeleton develops from a cartilage template that is prefigured by spatially patterned condensations of mesenchymal cells. The size and spacing of these condensations in the embryonic limbs of birds are mediated by a reaction-diffusion-adhesion network consisting of the matricellular proteins Gal-1A, Gal-8 and their glycosylated cell surface receptors. In cultures of limb precartilage mesenchymal cells we found that condensations appear simultaneously, which raised the question of how their formation is synchronized across distances greater than the characteristic wavelength of their spatial pattern. Since oscillatory dynamics of Hes1, a downstream target of Notch signaling, are involved in coordinating cell behavior during vertebrate somitogenesis, we explored whether they have a similar role in developing limb bud mesenchyme. Hes1 mRNA underwent oscillations with a periodicity of 6 hours during condensation formation in vitro. A mathematical model for the two-galectin pattern forming network, modified to incorporate periodicity in adhesive response of cells to Gal-1A, predicts that the spatiotemporal regularity of condensation formation is improved if the oscillator phase is synchronized across the culture. Treatment of cultures with DAPT, a pharmacological inhibitor of Notch signaling, led to elevation of both Gal-1A and -8 mRNA levels in vitro and in silico, suggesting that the Notch pathway is integral to the patterning network. DAPT predictably damped Hes1 oscillations and led to irregularly-sized and fused condensations in vitro. In developing limb buds *in ovo*, it led to spatially non-uniform Hes1 expression and fused and misshapen digits. Finally, the previously described sharpening effect of FGF2 on the condensation pattern was correlated with its enhancement of Hes1 synchronization. Together our experimental and computational results suggest that the two-galectin reaction-diffusion-adhesion network that patterns the avian limb skeleton is regulated by the Notch pathway. Moreover, global coordination of this pathway by synchronization of Hes1 oscillations across the tissue micromass *in vitro* or the digital plate *in vivo* refines and regularizes morphogenesis of the skeletal elements.

Keywords: Galectins; reaction-diffusion adhesion; morphogenetic field

Introduction

The appendicular skeleton in tetrapods is characterized by a stereotypical pattern that consists of an increase in number of bony elements arranged in series, along the proximodistal axis. Each bone is prefigured by a cartilaginous element that in turn differentiates from a cellular condensation: a tight aggregation of somatopleure-derived mesenchymal cells (Newman and Bhat, 2007). The digits in the tetrapod limb (collectively called the autopod) derive from such condensations, which arise spaced well-apart from each other. Investigations into the molecular mechanism(s) that pattern the pre-digit condensations: i.e., determine their size, number and spatial separation, have implicated a variety of molecules, including cell-cell adhesion proteins, extracellular matrix and matricellular proteins and their interacting partners, and diffusible morphogens (reviewed in (Newman and Bhat, 2007) and (Newman et al., 2008)). Of these, galectin-1A (Gal-1A) and galectin-8 (Gal-8) are, along with their putative receptors, the earliest proteins found to be expressed in a condensation-specific fashion within developing chicken limb mesenchyme (Bhat et al., 2011). They are also functionally involved in the patterning process: together they constitute an activator-inhibitor-adhesion reaction-diffusion network with well-characterized dynamics that determines the sizes and spacing of precartilage cell condensations in vitro and of digits in ovo (Bhat et al., 2011; Glimm et al., 2014).

Morphogenetic processes specified via reaction-diffusion-based mechanisms are constrained in the spatial scale of their activity by the local nature of diffusing interactors. For such systems to form reliable patterns over distances greater than their characteristic wavelengths (e.g., across the developing digital plate) they must incorporate one or more features that promote global coordination. The spatiotemporal synchronization of cell fates during development has been actively investigated over the last two decades in the context of vertebrate segmentation. Specifically, synchronized oscillations in the expression of genes belonging to signaling pathways such as Notch and Wnt constitute a molecular clock that appears to determine the periodicity of the

sequential formation of the somites that give rise to vertebrae and other tissues of the body (Aulehla and Pourquie, 2006). The frequency of the oscillations in expression of *hes1*, a gene encoding a transcription factor downstream of Notch in the unsegmented presomitic mesoderm, correlates with the formation of somites (Palmeirim et al., 1997). The chicken homolog of *hes1* (also known as *c-hairy1*), is also expressed within distal undifferentiated limb mesenchyme and its overexpression leads to shortening to skeletal elements (Vasiliauskas et al., 2003). The Notch pathway appears to be active within high-density micromass cultures of precartilage limb mesenchyme and its pharmacological inhibition led to increased size and irregular shapes of condensations and accelerated their formation (Fujimaki et al., 2006).

Here we present experimental evidence that the Notch signaling pathway is intrinsic to the two-galectin patterning network for precartilage condensation, and that the oscillatory expression of its downstream effector *hes1* is involved in the synchronized formation of condensations in vitro and the coordinated emergence of patterned digits in vivo. We incorporate the dynamics of phase synchronization on galectin expression within our mathematical model to provide a mechanistic understanding of how the entrainment of oscillations, both spontaneous and induced by the ectodermal morphogen FGF2, helps synchronize the spatial emergence of the condensation pattern and sharpen the boundaries of forming skeletal elements.

Results and Discussion

Limb precartilage mesenchymal cells condense simultaneously over millimeter distances in culture

When the digital plate mesenchyme of embryonic chicken limb buds is dissociated and cultured at a high density, cells begin aggregating within a few hours, forming regularly spaced foci (“protocondensations”) marked by the expression of the two galectins Gal-1A and Gal-8 (Bhat et al., 2011). These foci then mature into classically described precartilage condensations (Frenz et al., 1989; Paulsen and Solursh, 1988). We

tracked the formation of the condensations in time across high-density micromass culture (~3 mm diameter) with ~5% of the limb mesenchymal cells expressing H2B-GFP. Morphological condensations, first evident by fluorescence optics by about 48 h after the culture was initiated (as in similar cultures viewed by phase contrast microscopy), appeared nearly simultaneously across the entire micromass (Fig. 1, Movie S1). We have shown previously that the morphogenesis of individual condensations and the inhibition of formation of others in their immediate vicinity is dependent on local regulatory interactions between two galectins and their counterreceptors (Bhat et al., 2011; see also Lorda-Diez et al. (2011). Here, we find in addition that the morphogenetic events mediated by this network are synchronized across a non-local "morphogenetic field" (Gilbert and Sarkar, 2000; Levin, 2012), the culture micromass (as in Fig. 1 and Movie S1).

hes1 undergoes oscillation during condensation patterning in vitro

The evidence of temporal synchrony in condensation morphogenesis was suggestive of other cases of temporally coordinated pattern formation during animal development. During vertebrate somitogenesis, Notch signaling synchronizes *hes1* oscillations across the width of the lateral plate mesoderm, constituting each segmenting band of tissue as a morphogenetic field (Palmeirim et al., 1997). To test whether Notch-mediated Hes1 oscillations play a similar role in limb skeletal patterning, we assayed the gene expression of *hes1* in cultures of precartilage leg mesenchyme. When assayed at regular time points (with intervals ranging from 30 min -3 h), between 12 h and 24 h post-incubation (the time window within which the existence of early protocondensations within cultures is first evidenced), the expression of *hes1* was found to periodically rise and fall (Fig. 2A). Using the Lomb-Scargle algorithm, devised to quantify periodicity of a signal, the expression of *hes1* was found to oscillate with a periodicity of 6 h (Fig. 2B). When the interval between assay time points was decreased to 1 h or ½ h (to detect oscillations of potentially lower periodicities), the expression plots nevertheless showed signatures of oscillation with a periodicity of 6 h (Fig. S1).

An experimentally-based mathematical model predicts the role of phase synchrony in temporally coordinating condensation morphogenesis

Our observation of Hes1 cyclic expression led us to hypothesize that the synchronization of cell fates brought about through cell-cell interaction (e.g., the juxtacrine signaling mediated by Notch and its ligands) was important for the temporal uniformity in emergence of condensations in vitro and in vivo. We first tested this hypothesis computationally. To do this, we modified a mathematical model that had been constructed to represent the behavior of limb mesenchymal cells via their biosynthesis and adhesive/de-adhesive interactions with Gal-1A and Gal-8. Previously, this model was shown to accurately simulate the morphogenesis of condensations and the conditions of their formation on the basis of a reaction-diffusion-adhesion pattern-forming instability (Glimm et al., 2014). Here we have introduced an additional function to the model $\phi(x,t)$, representing the phase of the Hes1 cycle, and have made the cell response to the adhesive function of Gal-1A ("adhesion flux") depend on it (see further description of the model in Materials and methods). This extended model was devised in analogy to the hypothesized clock-and-wavefront mechanism of somitogenesis, where the epithelization of somatic plate mesoderm occurs only during a specific phase range of the Hes1 cycle (Palmeirim et al., 1997; (Aulehla and Pourquie, 2006; Chal et al., 2017).

We considered two scenarios: one in which the oscillations of the Hes1 molecular clock were in phase across the field of cells ('synchronized phase'), and the second where the initial phase distribution was random, but spatially correlated, leading to loss of synchrony of the phases of the molecular clock ('asynchronous phase'). We simulated the temporal emergence of cell density spatial distribution in both these cases (Fig. 3A, left top and Movie S2).

We observed that in the case of 'synchronized phase', a more regular spatial pattern in cell density peaks arose relative to the 'asynchronous phase' counterpart (Fig. 3A, left bottom). The regularity of patterns was quantified via a new measure, termed the

'relative maximum peak difference' (Fig. 3A right). This is the difference in density between the most dense condensation and the least dense condensation, i.e. the highest and the lowest peak in the cell density, relative to the highest density. This quantifies the uniformity of the pattern density across the different aggregation sites, with values close to zero indicate very regular patterns. While pattern formation was possible in both cases, leading to patterns with overall almost indistinguishable mean Fourier wavenumbers (Fig. S3A), the spatial regularity of the amplitude of cell density distribution was reproducibly diminished in the 'asynchronous phase' case (Fig. 3B).

Another measure of pattern regularity is the variance of the Fourier wavenumber of the cell density pattern, with smaller standard deviations indicating more regular patterns (e.g., a perfect sine wave having zero standard deviation). Here too, the standard deviation was slightly lower in the synchronized case, indicating greater regularity of those patterns (Fig. S3B). In fact, synchronizing the intracellular oscillatory phases after starting the simulations with random spatially correlated phases 'rescued' the uniformity in condensation patterning as well (Movie S3).

One crucial parameter was the galectin diffusion coefficient. The smaller the diffusion coefficient, the more irregular are the induced cell density patterns (Fig. 3B). We found that in the asynchronous phase case, the overall expression rates of the genes specifying both Gal-1A and Gal-8 predicted by the model were predicted to be mildly elevated compared to the synchronous phase case (Figs. 3C and 3D). The effect was more pronounced in simulations for which the galectin diffusion coefficients were smaller.

The γ-secretase inhibitor DAPT suppresses Hes1 expression and its oscillation and upregulates Gal-1A and Gal-8 mRNA levels

An assumption of our oscillation-enhanced mathematical model is that the galectin-based condensation patterning network is under the regulation of synchrony-inducing cell-cell communication. To test this, we treated limb micromass cultures with DAPT, an

inhibitor of the γ-secretase multiprotein complex. DAPT inhibits Notch signaling by impairing the cytoplasmic cleavage of the Notch intracytoplasmic domain but also can potentially affect the function of other cell signaling pathways in which presenilin-1-dependent intramembrane cleavage operates, such as those dependent on E-cadherin (Marambaud et al., 2002) or Eph-Ephrin (Tomita et al., 2006). In DAPT-treated micromass cultures there was a sustained decrease in the expression of the gene encoding Hes1, with no evidence of the oscillatory dynamics seen in control (compare Fig. 4A to Fig. 2A). As predicted by the model (Figs. 3C and D), the messenger RNA levels of genes coding for both Gal-1A and Gal-8 were found to be significantly elevated in cultures pretreated with DAPT (Fig. 4B).

Inhibition of γ-secretase alters condensation patterning dynamics in vitro and leads to disruption in digit morphologies in ovo

We analyzed the changes in condensation patterning associated with inhibition of γ-secretase by focusing on condensation number, condensation size and inter-condensation distance. Condensation number was decreased by DAPT, which could be accounted for by the fusion of neighboring condensations (Fig 5B). Frequency distributions of condensation sizes showed both increased smaller and bigger condensations (Fig. 5B left) whereas the distribution of intercondensation distance showed a left shift (Fig. 5B right), indicating irregular patterns of condensations upon DAPT treatment.

Our in vitro experiments suggest that γ-secretase-dependent Hes1 oscillations act to coordinate spatial patterning of condensations. We next sought to investigate if such an effect was also evidenced *in ovo*. Potential pattern refinement dependent on oscillator synchronization requires physical continuity throughout the morphogenetic field. We introduced tantalum foil barriers into prospective autopodial mesenchyme of avian wing buds and assayed for spatial expression of *hes1* by in situ hybridization. For each wing bud tested, the expression pattern was altered relative to the pattern in the contralateral counterpart (Fig. S3). The foil barriers typically led to disparate staining patterns on its

two sides, where the contralateral limb showed uniform high or low expression or a symmetrical expression pattern.

Earlier reports indicated that insertion of foil barriers at precondensation stages of autopodial development alters digit patterning (Rowe and Fallon, 1982). By our hypothesis this effect could be mediated by the disturbance of *hes1* expression synchrony resulting from this mechanical intervention. We used an alternative, biochemical means of perturbing *hes1* expression synchrony by (as above) injecting DAPT into the prospective autopod of developing wing buds. When evaluated post-chondrogenesis this treatment was seen to result in fusion between phalanges and other abnormalities in digit and proximal element morphologies (Fig. 5C).

FGF2, an ectodermal morphogen, sharpens *hes1* oscillations and inhibits galectin gene expression

In an earlier report, FGF2, a product of chick limb bud's dorsal and ventral ectoderm (distinct from FGF8, the main product of the developing limb's apical ectodermal ridge (AER); (Vogel et al., 1996)), was found to enhance the spacing between adjacent condensations, leading to a more demarcated pattern (Moftah et al., 2002) (Fig. 6A; a similar result was also seen with mouse micromasses; (Miura and Maini, 2004). We confirmed that this effect is potentially mediated by responses of the two-galectin network by noting a decrease in expression of genes encoding both Gal-1A and -8 in limb micromasses treated with FGF2 (Fig. 6B). However, given the multiscale complexities of galectin function in this system the reduction in expression of their genes provided little insight into the mechanism of pattern sharpening. We therefore looked at the effect of FGF2 treatment on *hes1* oscillations, the modulation of which had marked effects on condensation patterning (Fig. 5). We found that FGF2 treatment increased the amplitude of *hes1* oscillations (i.e., the fraction of cells in the micromass that were at the same *hes1* phase at the same time) (Fig. 6C). Thus a greater synchrony in phase of *hes1* is correlated with better-spaced (and hence more uniformly sized) condensations.

Conclusion

The concept of the morphogenetic field has been intermittently influential in developmental biology for close to a century (reviewed in (Gilbert et al., 1996) and Beloussov et al. (1997)). Joseph Needham, using a definition he attributed to C.H. Waddington, characterized a morphogenetic field as “a system of order such that the positions taken up by unstable entities in one part of the system bear a definite relation to the position taken up by other unstable entities in other parts of the system” (Needham (1937) p. 71). To biologists in the modern molecular and physics-informed period, the global coordination described has been variously attributed to competing signaling centers, the transcriptional effects of which are regulated by different extracellular morphogens (Zakin and De Robertis, 2010), electrical fields, in turn generated by and promoting, ion fluxes across cell boundaries (Levin, 2012), and quorum sensing in cell collectives mediated by morphogens and other transported signals (Widelitz and Chuong, 2016).

Our experimental observations, in combination with the oscillation-incorporated version of the theoretical model of Glimm et al. (2014) that we have presented in this paper strongly suggest that the synchronization of cell fates through γ-secretase-Hes1-dependent signaling results in spatiotemporal coordination of the patterning of digital condensations in micromasses in vitro and in the digital plate in situ. Synchronization of cellular oscillators does not require transport of materials like morphogens or ions between or through a field of cells, and is therefore an apt mechanism for the global coordination implied by classical notions of the morphogenetic field. The lack of dependence on molecular transport means that it can occur rapidly over linear distances of tens to hundreds of cells in tissues or yeast or bacterial suspensions, and both on theoretical (Strogatz, 2000) and experimental (Chen et al., 2017; Garcia-Ojalvo et al., 2004) grounds can occur by weak non-specific coupling between neighboring subunits that oscillate autonomously. Alternatively, synchronization may be a consequence of collective oscillations that only emerge when cells are in interaction with one another (O. Pourquié, personal communication).

Where oscillations of the gene regulatory factor *hes1* are synchronized, as occurs in the presegmental plate mesoderm of vertebrate embryos (Giudicelli et al., 2007) and in the digital plate mesenchyme described here, the levels of this transcriptional co-regulator are rendered identical across a developing primordium at any moment of development, eliminating a major source of randomness in spatially distant cells' responses to patterns of morphogenetic factors generated by resident mechanisms (e.g., diffusion gradients; reaction-diffusion processes). This phenomenon, evidenced in the remarkable simultaneity of emergence of condensations across a micromass culture (Movie S1), precisely fulfils the Needham-Waddington criterion of "unstable entities" in one part of the system being correlated with such entities in other parts of the system.

In an earlier study, *c-hairy 2*, a paralog of *hes1*, was shown to cycle with a 6h periodicity within developing chicken limb autopodial mesenchyme (Pascoal et al., 2007), suggesting that the cyclic gene expression dynamics we have observed may have multiple components. Neither our study nor the earlier one tested the direct involvement of Notch and its ligands on mediating synchronization of Hes gene expression, but the dependence on γ-secretase reported here, as well as the expression of Notch1 in the chicken digital plate at the appropriate stages (Williams et al., 2009) makes a strong circumstantial case for a role for this pathway. Moreover, in mouse limb micromass cultures the effect of DAPT in causing fusion of precartilage condensations (as reported here for chicken; Fig. 5A), was counteracted by exogenous Notch1 intracellular domain (Fujimaki et al., 2006). As a caveat, however, we note that DAPT also inhibits steps in the TGF-β pathway (Pazos et al., 2017), and that the responsiveness of limb bud mesenchyme to TGF-β with respect to expression of several chondrogenesis-related parameters is also cyclical (Leonard et al., 1991). So like the mesenchymal clock itself, the medium of its synchronization may also be multifactorial.

We suggest that the responsiveness of precartilage mesenchymal cells to elevated levels of Gal-1A (which are spatially organized by its interactions with Gal-8 in the reaction-diffusion adhesion network we have described) depends on the cells' Hes1

status. By synchronizing *hes1* gene expression the tissue ensures that the on-off responses in the digital plate will be sharp rather than noisy, leading to well-formed skeletal elements with smooth boundaries. In vitro, in the absence of nonuniformities such as Shh and Hox protein gradients, this synchrony has the effect of making all the condensations appear simultaneously.

The mechanism of action of one such vivo factor, FGF2, which is produced by the dorsal and ventral ectoderm and is thus present during the formation of skeletal elements in vivo, finds a natural interpretation in our results. As the limb bud elongates and proximally located cells escape the condensation-suppressive influence of the AER (Kosher et al., 1979) they begin to express FGF receptor 2, making them responsive to the pattern-sharpening effect of FGF2 (Moftah et al., 2002). By increasing the amplitude of Hes1 oscillations, FGF2 promotes field behavior of the mesenchyme, poising it to respond in orderly global fashion to the organizing effects of the two-galectin network, which it also appears to play a role in tuning.

Materials and methods

Chicken eggs

White Leghorn chicken fertilized eggs were obtained from Moyer's Chicks, Quakertown, PA. Eggs were incubated in a humidified incubator at 39°C for 5-8 days.

Micromass Cell culture

Primary high density micromass cultures were performed as described previously (Bhat et al., 2011). Briefly, mesenchymal tissue was dissected from the myoblast-free autopod field of leg and wing buds of stage 24 (Hamburger and Hamilton, 1951) chicken embryos (~4½ d of incubation), dissociated with trypLE Express solution (Gibco), filtered through Nytex 20-μm monofilament nylon mesh (Tetko, Briarcliff Manor, NY) and resuspended in medium for plating at 2.5×10^{5} cells per 10 μl spot. Cell spots were deposited in Costar 24 well tissue culture plates and allowed to attach for 1 h before the wells were flooded with 1 ml of serum-free defined medium (henceforth called DM,

(Paulsen and Solursh, 1988)): 60% Hams F12, 40% Dulbecco's modified Earle's Medium (DMEM), 5 µg/ml insulin, 100 nM hydrocortisone, 50 μg/ml L-ascorbic acid, 5 μg/ml chicken transferrin; Sigma). Medium was changed daily.

In experiments involving FGF2 treatment, cultures were incubated for specified time periods in media containing 200 ng/ml of FGF2 (R&D systems, Minneapolis, MN). In experiments to assay for effects of Notch signaling on galectins or synchronization of condensations, cultures were treated for specified time periods with 500 nM-5 μM DAPT (N- [N- (3,5-difluorophenacetyl-L-alanyl)]-S-phenylglycine t-butyl ester) (Sigma Aldrich).

Quantitative PCR

Total RNA was isolated from cells according to instructions included with the Absolutely RNA Microprep kit (Agilent) as described previously (Bhat et al., 2011). RNA isolated from cells from micromass cultures grown to specified time points or freshly dissected and dissociated 5d limb buds was quantitated with a Nanodrop ND-1000 spectrophotometer at 260 nM and used as template for the synthesis of cDNA. Comparative quantitative PCR (qPCR) was performed on the Mx3005P instrument (Stratagene) with Brilliant SYBR Green QPCR master mix (Stratagene). The amplification protocol for comparative quantitative PCR included the following steps: denaturation of anti-Taq-polymerase antibody at 95°C for 10 min, 40 amplification cycles (95°C for 30 sec, 55°C for 1 min, 72°C for 1 min) and melting the amplified DNA in order to obtain melting curve for the PCR product. Messenger RNA expression of the gene of interest was normalized to internal control gene β actin and analyzed by the $\Delta\Delta$Ct method (Livak and Schmittgen, 2001) . At least two biological replicates were prepared for all analyses.

Whole mount *in situ* hybridization

In situ hybridization was performed on whole embryos essentially as described (Acloque et al., 2008). cDNA for chicken Hes1 gene (kind gift from Dr. Olivier Pourquié) was inserted into pGEM-4Z vector (Promega), and linearized with *Eco*RI for synthesis of

labeled and antisense strands using SP6 polymerase and the digoxygenin-based DIG RNA labeling kit (Roche), or with *Hin*dIII for synthesis of the labeled sense strand using T7 polymerase and the DIG RNA labeling kit (Roche). All the prehybridization and post hybridization washes were performed using the BioLane HTI 16V tissue processing robot (Intavis Bioanytical Instruments, Koeln, Germany).

In ovo manipulation of wing buds

Chick embryos were incubated horizontally. On the third day, the eggs were candled to locate the position of the embryos and 3-4 ml of albumin was removed by puncturing the wide bottom of the egg with an 18-gauge needle attached to a syringe. On day 4 the shell overlying the embryo was carefully removed and the window in the egg sealed with sterile transparent tape. Between 5-6 days ~1μg of DAPT (2μg/ml in nuclease free PBS) was injected into the mesenchyme of the autopod field of the wing bud. Control embryos were injected with identical amounts of BSA. The egg was resealed and the embryos were allowed to grow for 2-3 more days.

Whole-mount skeletal preparation

Embryos at 8-9 d were washed in PBS and fixed in 5% trichloroactetic acid overnight. Embryos were stained 0.1% Alcian blue in acid alcohol overnight. Following destaining in acid alcohol overnight, embryos were dehydrated in absolute ethyl alcohol and cleared in methyl salicylate.

Statistics of pattern formation

Experiments that involved the inhibition of protein function and pharmacological treatment appeared to bring about a change in pattern formation. To quantitatively assess the effect of these agents on the condensation pattern, three parameters were assessed separately. These were condensation size, condensation number and intercondensation distance. The cultures were photographed under low magnification (2.5×) and the images were binarized using ImageJ software (http://www.rsb.info.nih.gov/ij/) (Schneider et al., 2012). The smallest condensation was chosen by eye from among all the culture pictures and was set as the threshold for the lower limit of

condensation size measurement. Image J was then used to automatically measure the number and sizes of condensations in each picture.

In order to measure inter-condensation distances, an arbitrary point was chosen on the boundary of each condensation. This point was then connected with the point on the boundary of the condensation that was farthest from it, such that the line connecting the two points lay within the condensation. Since most of the condensations were quasi-circular, the line joining the two points represented an approximation to the diameter of the condensation. The mid-point of this axis was taken to be the center of the condensation. The centers of the condensations were then connected to those of neighboring condensations and the intercondensation distances were measured.

The values of the condensation numbers, sizes and inter-condensation distances were represented as fold means +/-SEM. The difference between groups and controls was assessed by Student's t-test and taken to be significant if the p-value was <0.05.

The Lomb-Scargle algorithm

The Lomb Scargle algorithm is a statistical tool used to search for periodicity of fluctuating data when the data sets are incomplete or when the data collection is not stringently distributed over the entire period of data collection. The algorithm constructs a periodogram (a graph in which peaks indicate frequencies with significant periodicities) with known statistical properties. The L-S algorithm has advantages over other methods like Fast Fourier Transforms (FFTs) which require evenly sampled data, and has been used to identify oscillating genes involved in vertebrate segmentation (Dequeant et al., 2006).

Mathematical model

We used the following system of partial differential equations, which were adapted from Glimm et al. (2014), equations (4.2)-(4.4):

$$\frac{\partial R}{\partial t} = d_R \nabla^2 R - \nabla \cdot \left(\alpha(\phi) R \, K(R)\right)$$

$$\frac{\partial c_1^u}{\partial t} = d_{gal}\nabla^2 c_1^u + \nu(x,t)Rc_8^u - c_1^u$$

$$\frac{\partial c_8^u}{\partial t} = d_{gal}\nabla^2 c_8^u + \mu(x,t)(2c_1^u - 5)R - c_8^u$$

$$\frac{\partial \phi}{\partial t} = \omega + \left(d_R\frac{1}{R}\nabla R - \alpha(\phi)K(R)\right)\cdot\nabla\phi + \frac{d_R}{2}\nabla^2\phi$$

Here $R(x,t)$ is the cell density and $c_1^u(x,t)$ and $c_8^u(x,t)$ are the concentrations of diffusible CG-1A and CG-8, respectively, as functions of time t and position x. The intracellular Hes1 oscillations are modeled by an effective mean oscillation phase $\phi(x,t)$. The above equations model the diffusion and expression of galectins, as well as random motion of cells and cell-cell adhesion. The diffusion coefficient of the cell density was $d_R = 0.08$, while the galectin diffusion coefficient d_{gal} was varied around the standard value of $d_{gal} = 1$.The latter is modeled through an effective adhesion flux term (following Armstrong et al, 2006) given by

$$K(R) = (2c_1^u - 5)\int_{-0.04}^{0.04} R(x+s,t)(2c_1^u - 5)\frac{s}{|s|}ds.$$

To account for the oscillatory dynamics of Hes1, we consider the phase of the Hes1 cycle $\phi(x,t)$ as one of the variables. Its spatiotemporal evolution is governed by a constant rate of change ω, a small diffusion term to account for local interactions, and an advection term that models the effective transport of the phase with the cells (Jörg et al., 2016). The constant temporal rate of change ω was chosen as 8π, corresponding to a period of 6 hours.

Crucially, the effect of the state of Hes1 in its oscillatory cycle on the galectin genetic regulatory network was modeled via making the cell-cell adhesion flux dependent on the Hes1 phase $\phi(x,t)$. This is a 'high level' modeling approach: Since the details of the interactions are unknown, we incorporate their ultimate effect on cell movement rather than directly implementing their direct molecular effects. Specifically, we set

$$\alpha(\phi) = 17\ (1 + A \sin \phi(x,t))$$

where $0 \leq A \leq 1$ is a parameter that describes the relative amplitude of the oscillation.

Comparison to previous model

Our original model (Glimm et al., 2014) did not incorporate the Hes1 phase $\phi(x,t)$. There the main concern was the analysis of the galectin regulatory network and how and under what conditions it undergoes spatial symmetry breaking to form patterns of precartilage condensations. The present paper deals with a second order problem: the control of the regularity of patterns in space and time. Apart from incorporating an expression representing the experimentally inferred Hes1 oscillations, the present analysis also required more attention to the exact form of the initial conditions.

The simultaneous emergence of density peaks in Glimm et al. (2014) were a consequence of choosing initial conditions as random, spatially uncorrelated perturbations of a spatially homogeneous steady state of the cell density. The resulting initial conditions lacked a characteristic spatial scale, making them effectively uniform, which in turn led to a highly synchronous and uniform patterning. In the paper at hand, we use random initial conditions for both the cell density and the Hes1 phase, which are spatially correlated. (For the details of how the initial conditions were set up, see the next section.) This adds biological realism since it means that sites neighboring foci of elevated cell density have an increased likelihood of higher cell density as well. (For the details of how the initial conditions were set up, see the next section.) As a result, this yielded less regular condensation patterns in the absence of a global coordinating mechanism, as expected in any extended system employing only local interactions.

Simulations

In the first set of numerical simulations ('synchronized phase'), the initial phase $\phi(x,0)$ was chosen as the spatially constant value $\frac{\pi}{2}$, thus giving the spatially uniform phase $\phi(x,t) = \omega t + \frac{\pi}{2}$. In the second set of simulations ('asynchronous phase'), a random distribution for the initial phase $\phi(x,0)$ was generated as follows: Using a spatial

discretization of a one dimensional domain with N=1000 evenly spaced grid points, we first defined an 'influence function' I_n (for integer values n) such that $I_n = 1$ for $-4 < n < 4$, $I_n = 0$ for $n < -303$ or $n > 303$, a linear function with slope 1/300 for $-303 \leq n \leq -4$, interpolating between 0 and 1, and similarly a linear function of slope $-1/300$ for $4 \leq n \leq 303$, interpolating between 1 and 0. Starting with $\phi(x) = \pi/2$, we then choose a random point n^* and a number p which is -1 or +1 with equal probability and modify $\phi(x)$ by adding $p\frac{30\pi}{N} I_{n^*+n}$ to it, where this expression is to be understood cyclically. This process is repeated $15N$ times to generate a random phase $\phi(x)$ with mean $\pi/2$.
The system procedure was applied to produce the initial cell density $R(x)$, with the only differences being that the starting value was $R(x) = 1$ and the addition in each step was $p\frac{1}{N} I_{n^*+n}$, using the same notation as above.

The system was solved on the one-dimensional interval $[0,5]$ with periodic boundary conditions using a spatial discretization with N=2500 evenly spaced grid points and the method of lines with Matlab's ode45 algorithm, a variable step Runge-Kutta ODE solver. The resulting final cell densities were analyzed using the Discrete Fourier Transform. We also used a new measure we call the relative maximum peak difference, which is the difference between the largest local maximum and the smallest local maximum as a fraction of the largest local maximum. This is a measure of the regularity of the pattern; the larger this maximum peak difference, the less regular we may consider the pattern to be. We generated statistics with n=50 or n=75 runs of each set of simulations.

Table 1 Primer sets used for qRT-PCR

Gene of interest	Accession number PubMed	Forward primer (5' to 3')	Reverse primer (5' to 3')
β-actin	NM205518	CGGTACCAATTACTGGTGTTAGATG	GCCTTCATTCACATCTATCACTGG
Gal-1A	NM206.905.1	ATGGAGCAAGGACTGGTTGTTAC	TTAGCTGAACTTAATAGCTTTCACTTTAAAG
Gal-8	NM_001010843.1	ATGATGTCCTTGGATGGAC	CTACCAGCTCCTCACATC
Hes1	NM_001005848.1	GAGGCTAATACAGAGTTATGAGAC	AAGACCAGGAGATGAGAATGAC

References

Acloque, H., Wilkinson, D. G. and Nieto, M. A. (2008). In situ hybridization analysis of chick embryos in whole-mount and tissue sections. *Methods Cell Biol* **87**, 169-185.

Aulehla, A. and Pourquie, O. (2006). On periodicity and directionality of somitogenesis. *Anat Embryol (Berl)* **211 Suppl 7**, 3-8.

Beloussov, L. V., Opitz, J. M. and Gilbert, S. F. (1997). Life of Alexander G. Gurwitsch and his relevant contribution to the theory of morphogenetic fields. *Int J Dev Biol* **41**, 771-777; comment 778-779.

Bhat, R., Lerea, K. M., Peng, H., Kaltner, H., Gabius, H. J. and Newman, S. A. (2011). A regulatory network of two galectins mediates the earliest steps of avian limb skeletal morphogenesis. *BMC developmental biology* **11**, 6.

Chal, J., Guillot, C. and Pourquie, O. (2017). PAPC couples the segmentation clock to somite morphogenesis by regulating N-cadherin-dependent adhesion. *Development* **144**, 664-676.

Chen, C., Liu, S., Shi, X. Q., Chate, H. and Wu, Y. (2017). Weak synchronization and large-scale collective oscillation in dense bacterial suspensions. *Nature*.

Dequeant, M. L., Glynn, E., Gaudenz, K., Wahl, M., Chen, J., Mushegian, A. and Pourquie, O. (2006). A complex oscillating network of signaling genes underlies the mouse segmentation clock. *Science* **314**, 1595-1598.

Frenz, D. A., Jaikaria, N. S. and Newman, S. A. (1989). The mechanism of precartilage mesenchymal condensation: a major role for interaction of the cell surface with the amino-terminal heparin-binding domain of fibronectin. *Developmental biology* **136**, 97-103.

Fujimaki, R., Toyama, Y., Hozumi, N. and Tezuka, K. (2006). Involvement of Notch signaling in initiation of prechondrogenic condensation and nodule formation in limb bud micromass cultures. *Journal of bone and mineral metabolism* **24**, 191-198.

Garcia-Ojalvo, J., Elowitz, M. B. and Strogatz, S. H. (2004). Modeling a synthetic multicellular clock: repressilators coupled by quorum sensing. *Proc Natl Acad Sci U S A* **101**, 10955-10960.

Gilbert, S. F., Opitz, J. M. and Raff, R. A. (1996). Resynthesizing evolutionary and developmental biology. *Dev Biol* **173**, 357-372.

Giudicelli, F., Özbudak, E. M., Wright, G. J. and Lewis, J. (2007). Setting the tempo in development: an investigation of the zebrafish somite clock mechanism. *PLoS Biol* **5**, e150.

Glimm, T., Bhat, R. and Newman, S. A. (2014). Modeling the morphodynamic galectin patterning network of the developing avian limb skeleton. *Journal of theoretical biology* **346**, 86-108.

Hamburger, V. and Hamilton, H. L. (1951). A series of normal stages in the development of the chick embryo. *Journal of morphology* **88**, 49-92.

Kosher, R. A., Savage, M. P. and Chan, S. C. (1979). In vitro studies on the morphogenesis and differentiation of the mesoderm subjacent to the apical ectodermal ridge of the embryonic chick limb-bud. *Journal of embryology and experimental morphology* **50**, 75-97.

Leonard, C. M., Fuld, H. M., Frenz, D. A., Downie, S. A., Massagué, J. and Newman, S. A. (1991). Role of transforming growth factor-β in chondrogenic pattern formation in the

embryonic limb: stimulation of mesenchymal condensation and fibronectin gene expression by exogenous TGF-β and evidence for endogenous TGF-β-like activity. *Dev. Biol*. **145**, 99-109.

Levin, M. (2012). Morphogenetic fields in embryogenesis, regeneration, and cancer: non-local control of complex patterning. *Biosystems* **109**, 243-261.

Livak, K. J. and Schmittgen, T. D. (2001). Analysis of relative gene expression data using real-time quantitative PCR and the 2(-Delta Delta C(T)) Method. *Methods* **25**, 402-408.

Lorda-Diez, C. I., Montero, J. A., Diaz-Mendoza, M. J., Garcia-Porrero, J. A. and Hurle, J. M. (2011). Defining the earliest transcriptional steps of chondrogenic progenitor specification during the formation of the digits in the embryonic limb. *PloS one* **6**, e24546.

Marambaud, P., Shioi, J., Serban, G., Georgakopoulos, A., Sarner, S., Nagy, V., Baki, L., Wen, P., Efthimiopoulos, S., Shao, Z., et al. (2002). A presenilin-1/gamma-secretase cleavage releases the E-cadherin intracellular domain and regulates disassembly of adherens junctions. *The EMBO journal* **21**, 1948-1956.

Miura, T. and Maini, P. K. (2004). Speed of pattern appearance in reaction-diffusion models: implications in the pattern formation of limb bud mesenchyme cells. *Bull Math Biol* **66**, 627-649.

Moftah, M. Z., Downie, S. A., Bronstein, N. B., Mezentseva, N., Pu, J., Maher, P. A. and Newman, S. A. (2002). Ectodermal FGFs induce perinodular inhibition of limb chondrogenesis in vitro and in vivo via FGF receptor 2. *Developmental biology* **249**, 270-282.

Needham, J. (1937). Chemical aspects of morphogenetic fields. In *Perspectives in Biochemistry* (ed. J. Needham & D. E. Green), pp. 66-80. London: Cambridge University Press.

Newman, S. A. and Bhat, R. (2007). Activator-inhibitor dynamics of vertebrate limb pattern formation. *Birth Defects Res C Embryo Today* **81**, 305-319.

Newman, S. A., Christley, S., Glimm, T., Hentschel, H. G., Kazmierczak, B., Zhang, Y. T., Zhu, J. and Alber, M. (2008). Multiscale models for vertebrate limb development. *Curr Top Dev Biol* **81**, 311-340.

Palmeirim, I., Henrique, D., Ish-Horowicz, D. and Pourquié, O. (1997). Avian hairy gene expression identifies a molecular clock linked to vertebrate segmentation and somitogenesis. *Cell* **91**, 639-648.

Pascoal, S., Carvalho, C. R., Rodriguez-Leon, J., Delfini, M. C., Duprez, D., Thorsteinsdottir, S. and Palmeirim, I. (2007). A molecular clock operates during chick autopod proximal-distal outgrowth. *Journal of molecular biology* **368**, 303-309.

Paulsen, D. F. and Solursh, M. (1988). Microtiter micromass cultures of limb-bud mesenchymal cells. *In Vitro Cell Dev Biol* **24**, 138-147.

Pazos, M. C., Abramovich, D., Bechis, A., Accialini, P., Parborell, F., Tesone, M. and Irusta, G. (2017). Gamma secretase inhibitor impairs epithelial-to-mesenchymal transition induced by TGF-beta in ovarian tumor cell lines. *Molecular and cellular endocrinology* **440**, 125-137.

Rowe, D. A. and Fallon, J. F. (1982). Normal anterior pattern formation after barrier placement in the chick leg: further evidence on the action of polarizing zone. *J Embryol Exp Morphol* **69**, 1-6.

Schneider, C. A., Rasband, W. S. and Eliceiri, K. W. (2012). NIH Image to ImageJ: 25 years of image analysis. *Nature methods* **9**, 671-675.

Strogatz, S. H. (2000). From Kuramoto to Crawford: exploring the onset of synchronization in populations of coupled oscillators. *Physica D: Nonlinear Phenomena* **143**, 1-20.

Tomita, T., Tanaka, S., Morohashi, Y. and Iwatsubo, T. (2006). Presenilin-dependent intramembrane cleavage of ephrin-B1. *Molecular neurodegeneration* **1**, 2.

Vasiliauskas, D., Laufer, E. and Stern, C. D. (2003). A role for hairy1 in regulating chick limb bud growth. *Developmental biology* **262**, 94-106.

Vogel, A., Rodriguez, C. and Izpisua-Belmonte, J. C. (1996). Involvement of FGF-8 in initiation, outgrowth and patterning of the vertebrate limb. *Development* **122**, 1737-1750.

Widelitz, R. and Chuong, C. M. (2016). Quorum sensing and other collective regenerative behavior in organ populations. *Curr Opin Genet Dev* **40**, 138-143.

Williams, R., Nelson, L., Dowthwaite, G. P., Evans, D. J. and Archer, C. W. (2009). Notch receptor and Notch ligand expression in developing avian cartilage. *Journal of anatomy* **215**, 159-169.

Zakin, L. and De Robertis, E. M. (2010). Extracellular regulation of BMP signaling. *Curr Biol* **20**, R89-92.

Figure Legends

Figure 1. In vitro precartilage mesenchymal condensations emerge in spatiotemporal coordination. Time lapse fluorescent micrographs of a high density micromass culture of precartilage limb mesenchymal cells with ~5% cells expressing H2B-GFP. Condensations of mesenchymal cells appear simultaneously across the field of view suggesting that condensation morphogenesis is coordinated across the micromass.

Figure 2. Gene expression of Hes1 undergoes oscillation in condensing mesenchymal cells within high density micromasses. Assay for Hes1 gene expression within developing limb bud micromass cells using Real Time quantitative PCR shows an oscillatory temporal pattern (A). Analysis using Lomb-Scargle algorithm reveals a periodicity of 6 hours for oscillation of Hes1 mRNA levels. Error bars represent S.E.M. *p < 0.05.

Figure 3: A model integrating oscillation in cell state with a reaction-diffusion-adhesion-based patterning mechanism predicts a role for synchronization in the spatiotemporal coordination of condensations. A: Sample simulation. Top: Cell density of synchronous phase (blue) and sine of the Hes1 phase (red). Bottom: Cell density and sine of the Hes1 phase for asynchronous (random) phase. Note that the bottom cell density appears less regular. B: Relative maximum peak difference as a function of time based on N=75 simulations of synchronized Hes1 phases (solid line) and asynchronous Hes1 phases (dashed) for four different values of the galectin diffusion coefficient $d_{gal} = 0.1, 0.5, 1, 10$ as a fraction of the standard value used in simulations. The relative amplitude of the effect of the Hes1 oscillations on the cell-cell adhesion flux coefficient was *A=0.3.* The plot was temporally smoothed with a Loess algorithm with a span of 30% of the time interval. C, D: Predicted abundance of galectins CG-1A and CG-8 over time. Inset: Detail for time 1.9 d≤t ≤ 2.0 d predicts a mild increase in Gal-1A and Gal-8 abundance when Hes1 phases are synchronous relative to the condition when the phases are asynchronous. This difference is only observed when galectin diffusion coefficient $d_{gal} = 0.1$. Key (bottom) shows the

temporal dynamics of parameters measured in B, C and D at different galectin diffusion coefficients and when phases are synchronous (solid lines) versus asynchronous (dashed lines).

Figure 4. The γ-secretase inhibitor DAPT enhances the gene expression of Gal-1A and Gal-8. Treatment of limb micromass cultures with DAPT results in a damping in the expression of Hes1 mRNA when assessed between 15-24 hours post initiation of culture, using RTqPCR (A). Treatment with DAPT increased expression of Gal-1A (left) and Gal-8 (right) when assayed relative to untreated micromasses at 9 hours and 18 hours post culture initiation. Error bars represent S.E.M. *p < 0.05.

Figure 5. DAPT disrupts condensation patterning in culture and leads to dysmorphic digits in ovo Treatment of precartilage limb micromasses with □-secretase inhibitor DAPT increased fusion of condensations (A) with a resultant significant change in intercondensation distance and mean condensation size ($p<0.05$) (B) Depicted here are frequency distributions of condensation sizes and numbers which change upon treatment with DAPT. (C) In ovo, injection of DAPT into developing wing autopodium resulted in alteration in digit morphologies with fusions between digital elements.

Figure 6. Exogenous treatment with FGF2 imrpoves the condensation pattern and enhances Hes1 oscillatory amplitude. Treatment of micromasses with FGF2 led to a more demarcated pattern with pronounced intercondensation spacing (A). In addition, mRNA levels of Gal-1A and Gal-8 are decreased relative to untreated controls at 9h (B) and the amplitude of *hes1* oscillation were increased (C) Error bars represent S.E.M. *p < 0.05.

.

Supplementary Figures

Figure S1. Hes1 expression in cell cultures every half hour (above) and one hour (below) show incomplete signatures of oscillation, whose predicted time period is 6 h.

Figure S2. Comparison of one dimensional numerically simulated condensation patterns. Data based on simulations of the case of synchronized Hes1 phases (solid line) and asynchronous Hes1 phases (dashed) for four different values of the galectin diffusion coefficient $d_{gal} = 0.1,0.5,1,10$ as a fraction of the standard value used in simulations. The relative amplitude of the effect of the Hes1 oscillations on the cell-cell adhesion flux coefficient was $A = 0.3$. The plots in SB were temporally smooth with a Loess algorithm with a span of 30% of the time interval. **A:** Mean Fourier wavenumber as a function of time. **B:** Standard deviation of the Fourier wavenumber as a function of time. Inset: Detail for time $1.4d \leq t \leq 1.8d$

The results show that the difference between the synchronized and random phase cases is relatively small. The mean wavenumber of the resulting patterns at the end of the simulated time is hardly dependent on whether the Hes1 phases are synchronous or not (A1). However, the synchronous simulations show a somewhat smaller standard deviation (A2), indicating more regular patterns in the case of synchronous oscillations. (Compare to Figure 3B.) The same set of simulations as for Figure 3 were used.

Figure S3: Introducing physical discontinuity by tantalum foil insertion results in a perturbation in the spatial pattern of Hes1 gene expression in limb mesenchyme.

Movie S1: Time-lapse video of a high-density leg bud micromass culture photographed using fluorescence optics. The cell layer, which is confluent from the start, contains a subpopulation (approximately 5% of the total) that were electroporated with a DNA plasmid directing the expression of H2B-GFP. Precartilage condensations emerge in a synchronous fashion over the entire 2.5 mm diameter culture (the field of view in the video is about 2 mm wide) becoming clearly visible by the end of two days and forming cartilage nodules over the next day and a half.

Movie S2: Comparison of two simulations of cell condensation in one spatial dimension using the mathematical model described in the "Materials and Methods" section. The simulated time is between 0 days and 2.0 days. The blue curve shows the cell density $\mathrm{R}(\mathrm{t},\mathrm{x})$ as a function of space, normalized so that the initial uniform density is 1. The red curve shows the fraction $0.3\ \sin\phi(\mathrm{t},\mathrm{x})$ of the sine of the Hes1 phase. Top panel: Synchronized phases. Bottom panel: Asynchronous phases. The random initial cell density is the same for both panels. The galectin diffusion coefficient is 1. The condensation pattern emerges more synchronously in the synchronized phase case and the resulting pattern is more uniform. (Other parameters: $d_{gal} = 1, A = 0.3$)

Movie S3: Comparison of two simulations of cell condensation in one spatial dimension using the mathematical model described in the "Materials and Methods" section. Parameters and presentation is the same as in movie S2. The initial simulated time period of 0.4 days is the same for both panels. At that point in time, the phase $\phi(\mathrm{t},\mathrm{x})$ is spatially synchronized in the bottom ('rescue') panel. The condensation pattern emerges more synchronously in this 'rescued' panel and the resulting pattern is more uniform.

Figure 1

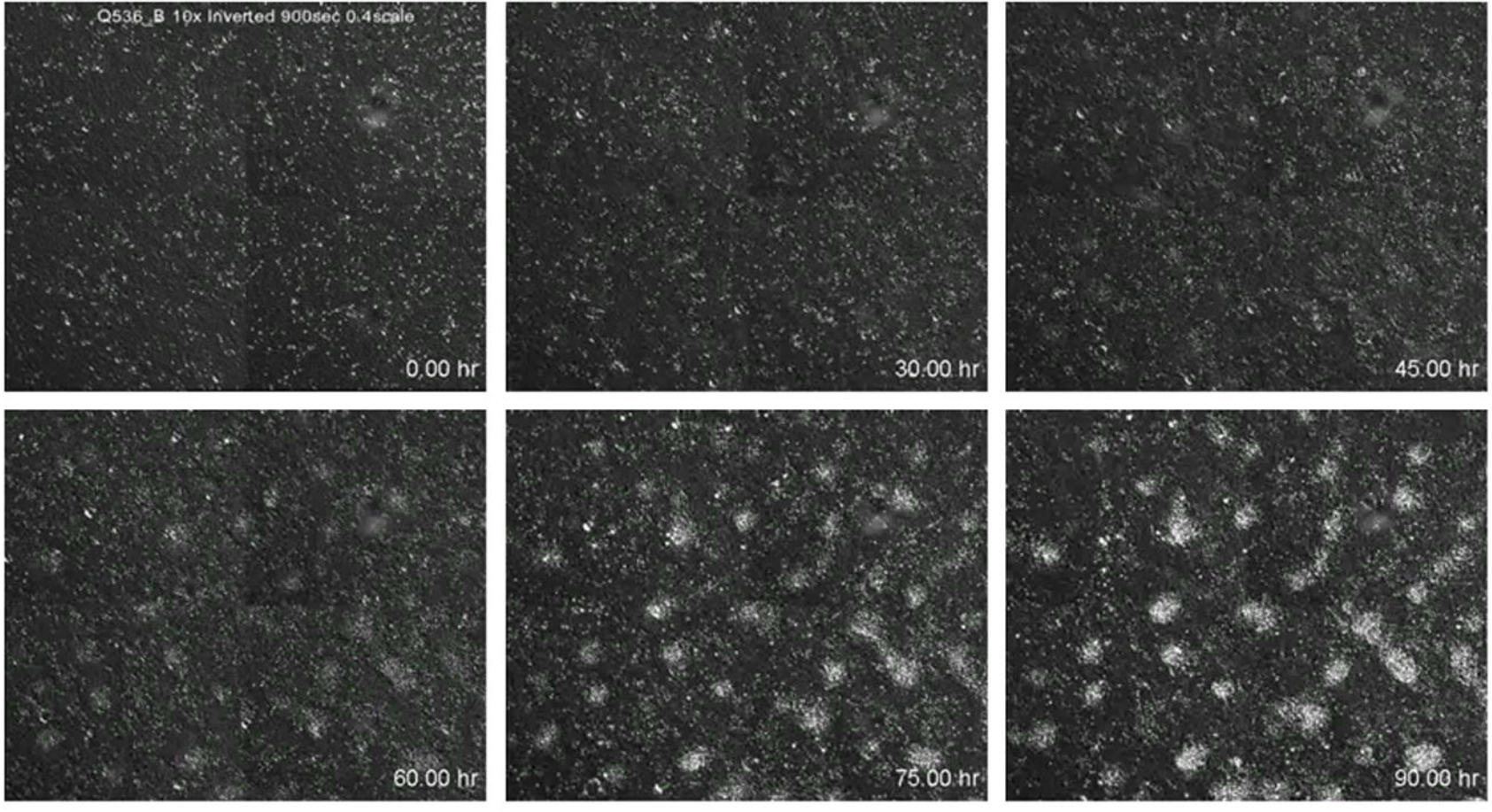
Q536_B 10x Inverted 900sec 0.4scale
0.00 hr
30.00 hr
45.00 hr
60.00 hr
75.00 hr
90.00 hr

Figure 2

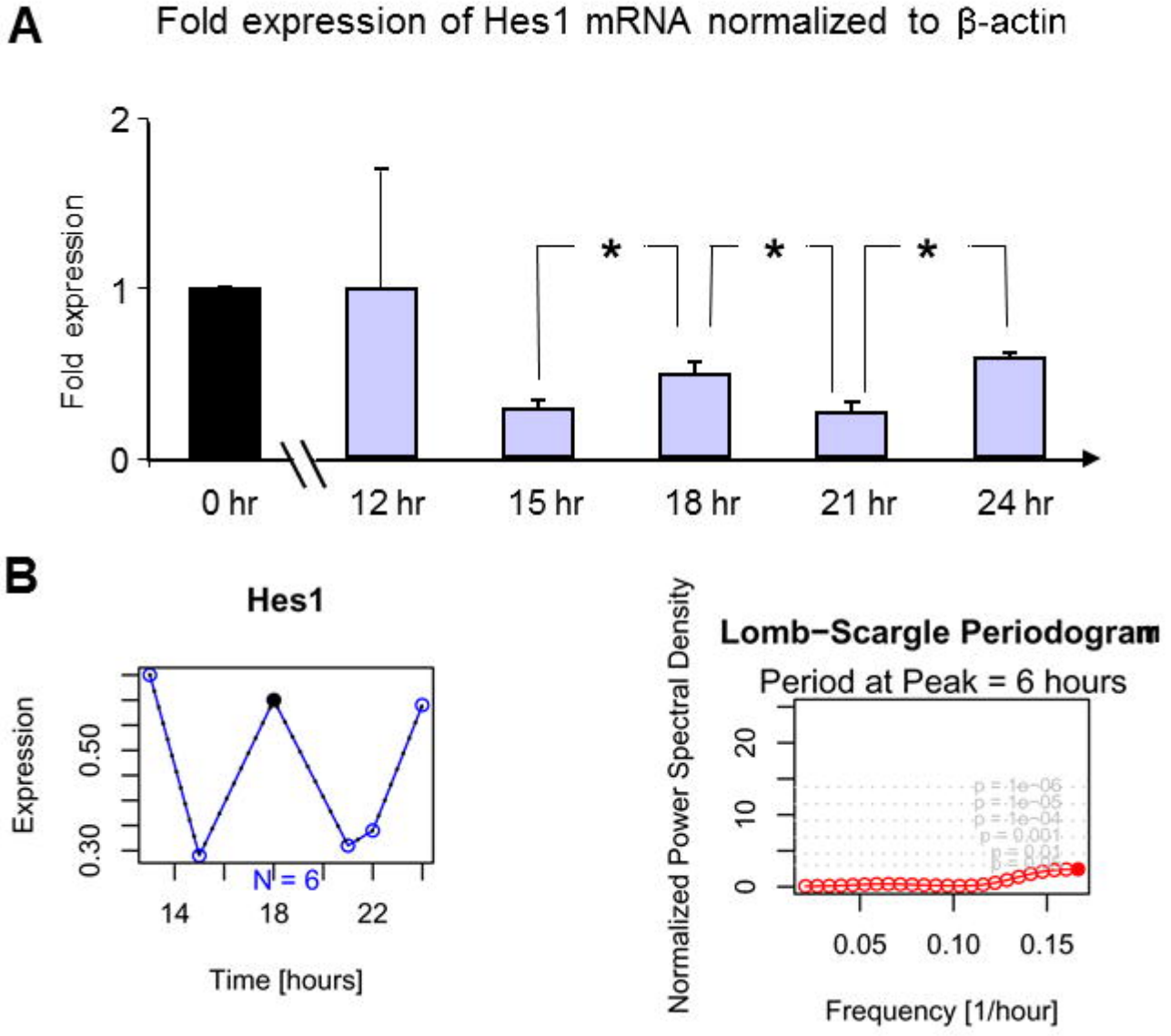
A
Fold expression of Hes1 mRNA normalized to β-actin
Fold expression
2
1
0
*
*
*
0 hr
12 hr
15 hr
18 hr
21 hr
24 hr
B
Hes1
Expression
0.30
0.50
N = 6
14
18
22
Time [hours]
Lomb−Scargle Periodogram
Period at Peak = 6 hours
Normalized Power Spectral Density
0
10
20
p = 1e−06
p = 1e−05
p = 1e−04
p = 0.001
p = 0.01
0.05
0.10
0.15
Frequency [1/hour]

Figure 4

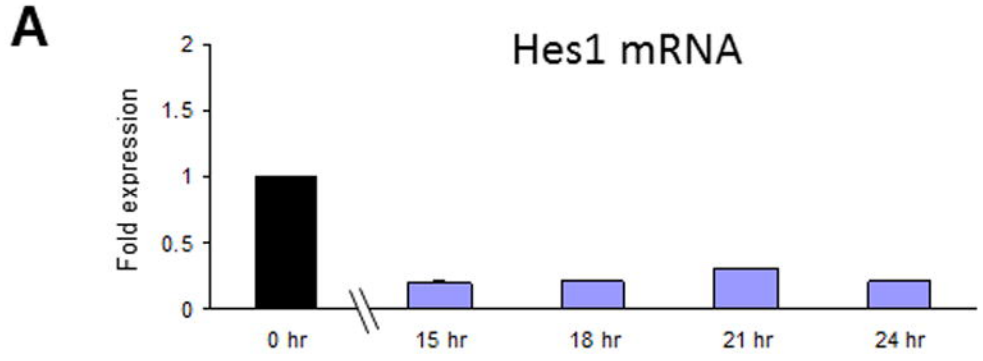
A
Hes1 mRNA
Fold expression
2
1.5
1
0.5
0
0 hr
15 hr
18 hr
21 hr
24 hr

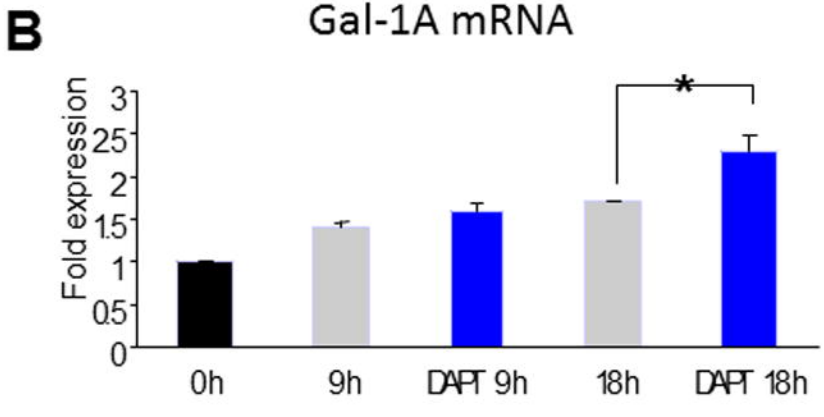
B
Gal-1A mRNA
Fold expression
3
2.5
2
1.5
1
0.5
0
*
0h
9h
DAPT 9h
18h
DAPT 18h

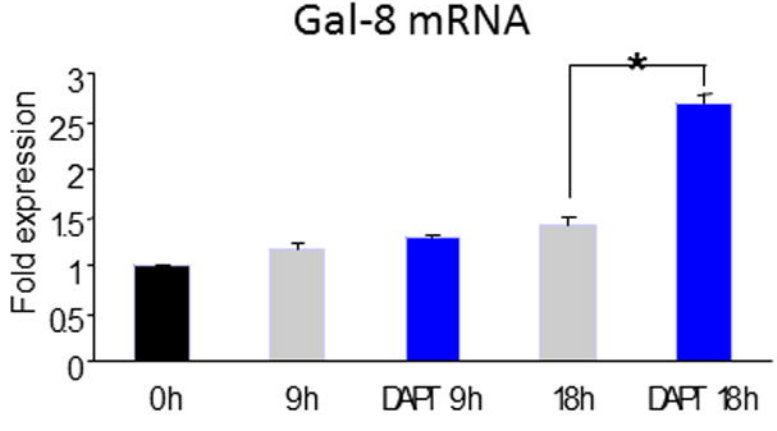
Gal-8 mRNA
Fold expression
3
2.5
2
1.5
1
0.5
0
*
0h
9h
DAPT 9h
18h
DAPT 18h

Figure 5

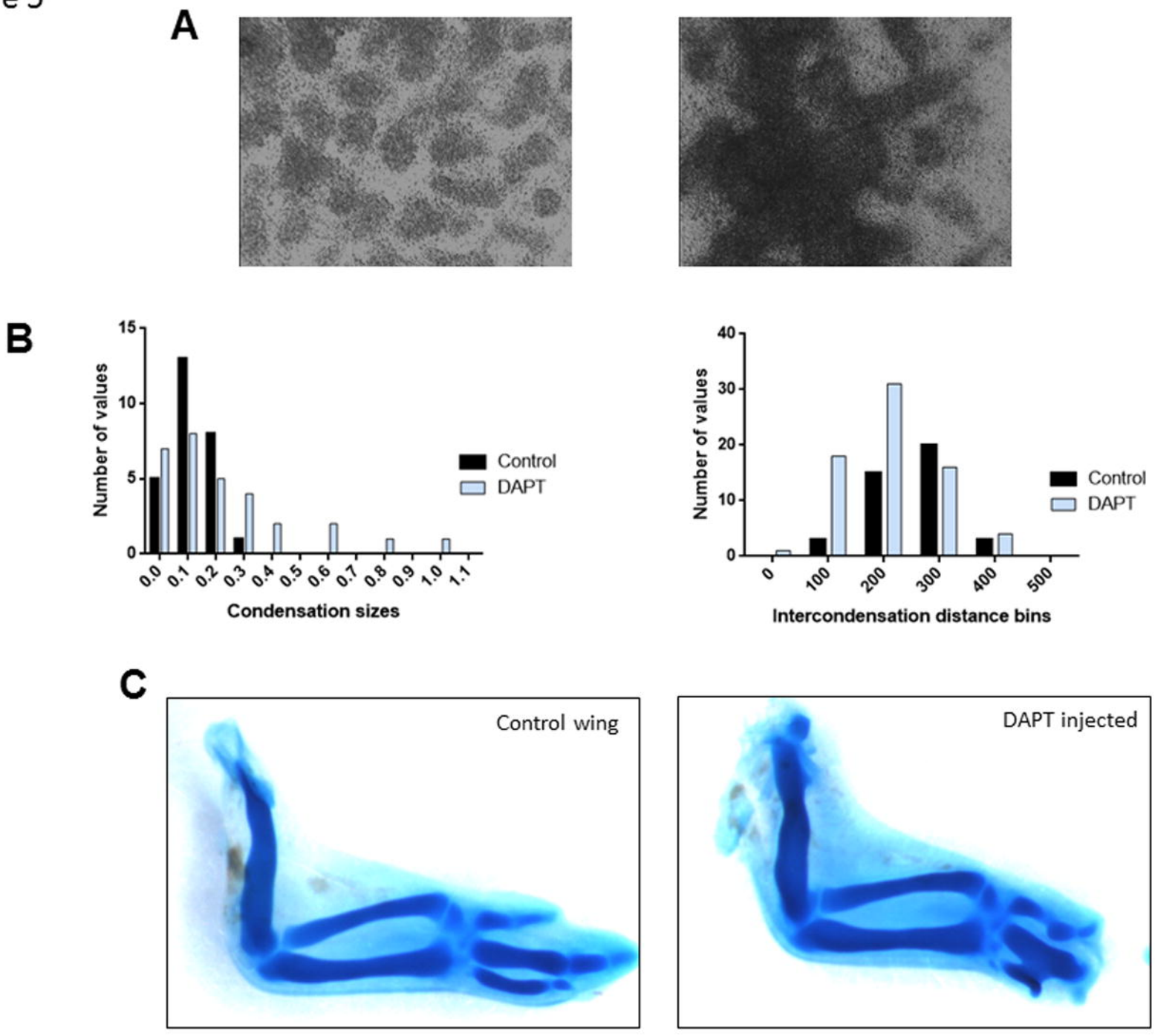
A
B
Number of values
15
10
5
0
0.0
0.1
0.2
0.3
0.4
0.5
0.6
0.7
0.8
0.9
1.0
1.1
Condensation sizes
Control
DAPT
Number of values
40
30
20
10
0
0
100
200
300
400
500
Intercondensation distance bins
Control
DAPT
C
Control wing
DAPT injected

Figure 6

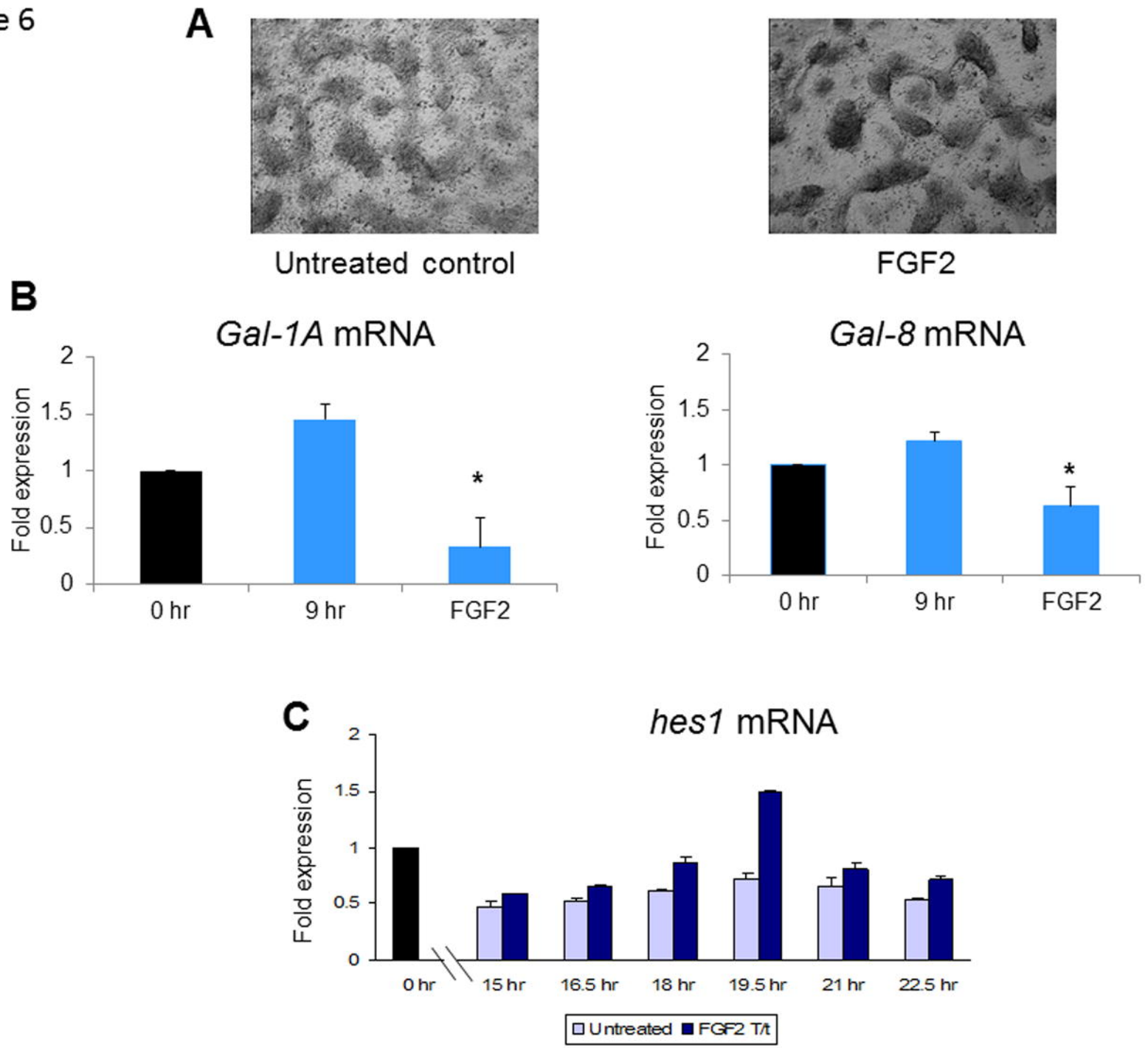
A
Untreated control
FGF2
B
Gal-1A mRNA
Fold expression
2
1.5
1
0.5
0
0 hr
9 hr
FGF2
*
Gal-8 mRNA
Fold expression
2
1.5
1
0.5
0
0 hr
9 hr
FGF2
*
C
hes1 mRNA
Fold expression
2
1.5
1
0.5
0
0 hr
15 hr
16.5 hr
18 hr
19.5 hr
21 hr
22.5 hr
Untreated
FGF2 T/t

Figure 3

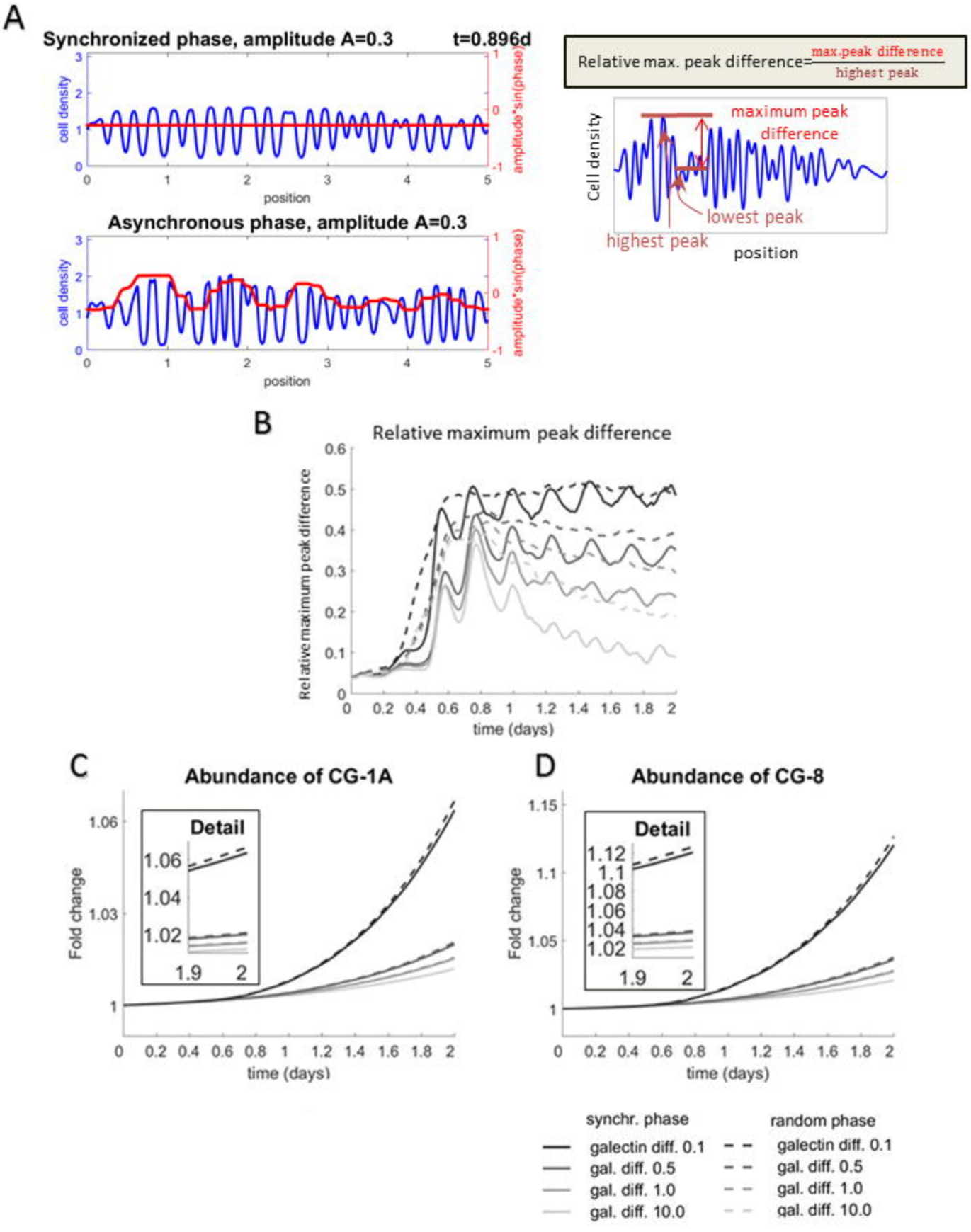
A
Synchronized phase, amplitude A=0.3
t=0.896d
cell density
amplitude*sin(phase)
position
Asynchronous phase, amplitude A=0.3
Relative max. peak difference=max.peak difference / highest peak
maximum peak difference
lowest peak
highest peak
Cell density
position
B
Relative maximum peak difference
Relative maximum peak difference
time (days)
C
Abundance of CG-1A
Detail
Fold change
time (days)
D
Abundance of CG-8
Detail
Fold change
time (days)
synchr. phase
random phase
galectin diff. 0.1
gal. diff. 0.5
gal. diff. 1.0
gal. diff. 10.0
galectin diff. 0.1
gal. diff. 0.5
gal. diff. 1.0
gal. diff. 10.0